# Effect of Dissolved Oxygen on Flow-Accelerated Corrosion in Neutral and Alkaline Solutions

**Kazutoshi FUJIWARA[1], Kimitoshi YONEDA[2], Fumio INADA[3]**

[1]*Central Research Institute of Electric Power Industry, Yokosuka, Japan,*
*fujik@criepi.denken.or.jp*
[2]*Central Research Institute of Electric Power Industry, Yokosuka, Japan,*
*yone@criepi.denken.or.jp*
[3]*Central Research Institute of Electric Power Industry, Yokosuka, Japan,*
*inada@criepi.denken.or.jp*

Abstract: Understanding of flow accelerated corrosion (FAC) is very important for wall-thinning management in commercial power plants. In our previous study, we proposed an FAC model taking into consideration the diffusion of soluble species. However, the effect of dissolved oxygen (DO) on FAC has not been clarified sufficiently. To improve the model, it is necessary to qualitatively evaluate the effect of DO on FAC. In the present study, the effect of DO on the FAC rate was experimentally evaluated in neutral and alkaline solutions at 413 and 453 K. In the neutral ($pH_{298K}$ 7.0) and alkaline solutions ($pH_{298K}$ 9.2) at 413 K, the FAC was suppressed when the DO concentration was increased to more than 55 and 12 ppb, respectively. At 453 K, the DO concentration required for FAC suppression was more than 30 and 4 ppb in the neutral solution ($pH_{298K}$ 7.0) and alkaline solution ($pH_{298K}$ 9.8), respectively. The DO concentration required for FAC suppression was not affected by the flow velocity according to the result predicted by the FAC model. However, it was higher than the value predicted by the FAC model. It is assumed that the discrepancy between the experimental and the predicted results was caused by the uncertainty in the diffusion coefficient of soluble iron and that the diffusion coefficient was affected by the distribution of soluble ferrous species. The modification of the diffusion coefficient improved predictive accuracy of FAC rate.

Keywords: flow-accelerated corrosion, feed water piping, carbon steel, dissolved oxygen, diffusion coefficient

## Introduction

Understanding of flow-accelerated corrosion (FAC) is very important for wall-thinning management in commercial power plants. FAC is observed in a wide range of temperatures. The maximum FAC rate of carbon steel under a single-phase flow is observed at approximately 403−423 K in neutral and alkaline solutions ($7 < pH_{298\ K} < 9$) [1, 2]. The FAC rate decreases with increasing pH and is less than 0.01 mm·y$^{-1}$ at $pH_{298\ K} = 9.5$ [2, 3]. The FAC rate of carbon steels is markedly decreased by the addition of more than 40 and 2 μg·kg$^{-1}$ oxygen in neutral and alkaline solutions, respectively [4−8]. Under oxidizing conditions, $Fe_2O_3$ rather than $Fe_3O_4$ becomes stable in the solid phase and the solubility of Fe decreases. The solubility and diffusion of the soluble species are expected to be the most important factors in FAC. In our previous study, a novel model of the effect of chemical on FAC (FAC model) under a steady-state condition was developed by considering the diffusion of soluble iron and chromium species, dissolved hydrogen, and dissolved oxygen. A formula to evaluate the critical dissolved oxygen (DO) concentration for FAC suppression was also derived. However, there was some uncertainty in the diffusion coefficient of soluble iron in the model. To verify the model, it is very important to understand the combined effects of each parameter, such as DO concentration and pH, on FAC.

In the present study, the effects of the DO concentration on the FAC rate of carbon steel were evaluated by using high temperature loop equipment with an on-line corrosion-monitoring system. The experimental FAC rates were compared with the results calculated by the FAC model, which was constructed by considering the solubility and diffusion of soluble species.

## **Experimental**

### FAC test using a high-flow-rate loop system

Figure 1 shows a schematic diagram of the FAC loop. This facility allows on-line monitoring of the wall-thinning rate of carbon steel piping by using tube probes (Fig. 2). The tube probes were made from carbon steel (STPT 480), whose chemical composition is given in Table 1.

The test solutions in the main tank are fed into tube probes with a high velocity. A heat exchanger and heater are installed before the test sections to heat the solutions. Downstream of the test section, the solution is cooled to room temperature in the heat exchanger and the cooler. The experimental conditions of the FAC test are shown in Table 2. The first and third tests were carried out in deionized neutral water, and the second and fourth tests were carried out in ammonia ($NH_3$) solution with $pH_{298\ K}$ values of 9.2 and 9.8, respectively. The temperature of the solution at the test section was controlled to 413 or 453 K. $NH_3$ was injected into the feed water from the chemical injection tank. The DO concentration was controlled in the main tank and increased in a step wise manner.

In the on-line monitoring of the wall-thinning rate of the tube probes, the wall-thickness was calculated from the electrical resistance of the tube probes [9]. Two pairs of silver wire were soldered to the tube probes. One pair was used to supply direct current and the other was used for potential drop measurements. The progress of the wall-thinning by FAC increased the electric resistance ($R_s$) of the tube probes. The inner diameter ($r_i$) of the tube probe was calculated by

$$r_i = (r_o^2 - \rho_s \cdot L_s \cdot \pi^{-1} \cdot R_s^{-1})^{1/2}. \tag{1}$$

Here, $\rho_s$ is the resistivity of the specimen, $L_s$ is the distance between soldering points, and $r_o$ is the outer diameter.

Table 1        Chemical composition of specimens used for FAC test.

(wt%)

| Material | C | Si | Mn | P | S | Cr | Mo | Fe |
|---|---|---|---|---|---|---|---|---|
| STPT 480 | 0.25 | 0.24 | 0.80 | 0.017 | 0.010 | 0.001 | <0.01 | Bal. |

Table 2        Experimental conditions of FAC test.

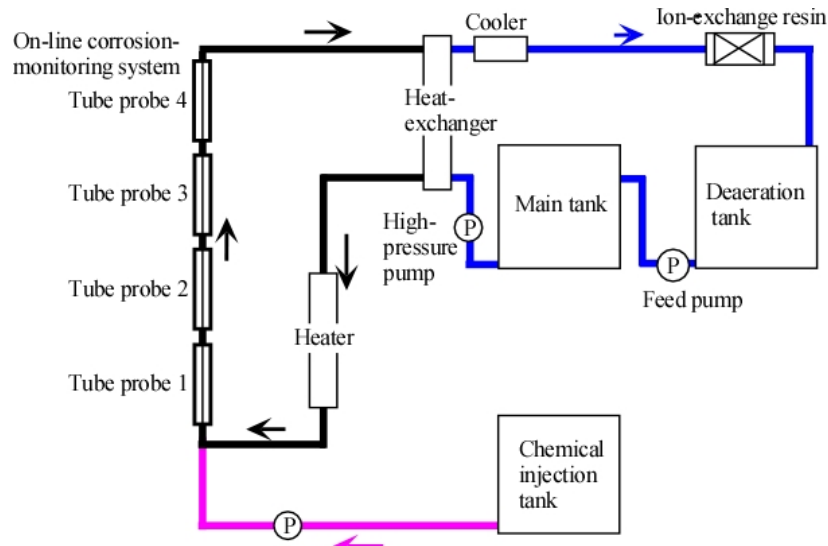| Test | Temp. (K) | $pH_{298K}$ | Velocity (m/s) |
|---|---|---|---|
| 1st | 413 | 7 | 5, 12, 30 |
| 2nd | 413 | 9.2 | 5, 12, 30 |
| 3rd | 453 | 7 | 5, 30 |
| 4th | 453 | 9.8 | 5, 30 |

Figure 1        The schematic diagram of the FAC loop.
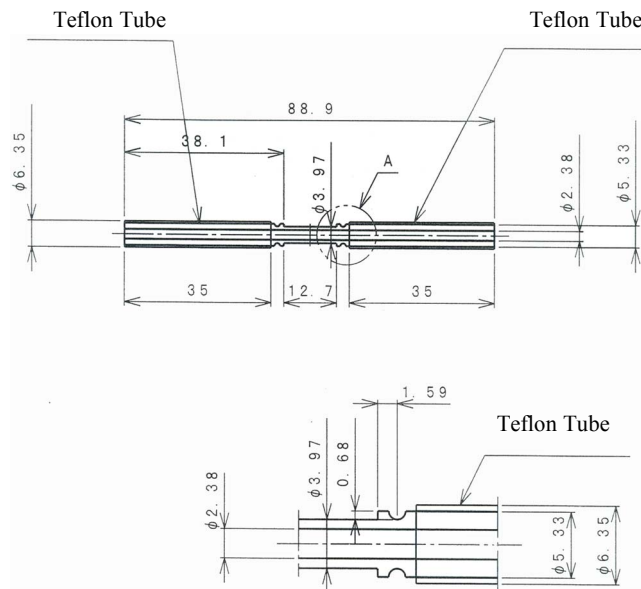


Figure 2        Schematic diagram of tube probes.

FAC model

Figure 3 shows our FAC model, which is based on the following assumptions [10−12].

1) Thermodynamic equilibrium is achieved in the layer at the material/solution interface (saturated layer).

2) The soluble species diffuse between the bulk solution and saturated layer through the diffusion layer. The rate-determining step of FAC is the diffusion of the soluble iron.

In the case of a difference between the concentration at the saturated layer ($C_{s,M}$) and the concentration of the bulk solution ($C_{\infty,M}$), the soluble species M diffuses from the material/solution interface to the bulk solution in accordance with Fick's law. The flux of the soluble species ($J_M$) is proportional to the concentration difference ($C_{s,M} - C_{\infty,M}$). Therefore, $J_M$ is expressed as

$$J_M = 2\, D_M \cdot \delta^{-1} \cdot (C_{s,M} - C_{\infty,M}). \tag{2}$$

3

Here, $D_M$ is the diffusion coefficient of M and $\delta$ is the thickness of the diffusion layer. The thickness of the diffusion layer can be defined in terms of Sherwood number, $Sh$, as follows:

$$\delta = 2\,d \cdot Sh^{-1}. \tag{3}$$

Here, $d$ is a characteristic length. In the case of a tube, $d$ is equal to the inner diameter of the tube. From the Chilton−Colburn analogy of mass and heat transfer, $Sh$ is expressed in terms of the Reynolds number ($Re$) and Schmidt number ($Sc$) [13] as
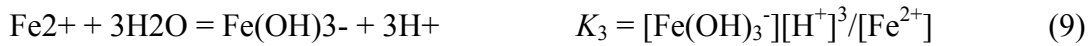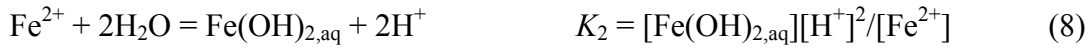
$$Sh = 0.0395\,Re^{0.75} \cdot Sc^{1/3}. \tag{4}$$

The iron concentration in the saturated layer is equal to the thermodynamic solubility of iron ($S_{Fe}$). It is convenient and conservative to assume that the soluble iron concentration in the bulk solution is zero. The FAC rate ($J_{FAC}$) can be expressed by

$$J_{FAC} \approx 2\,D_{Fe} \cdot \delta^{-1} \cdot S_{Fe}. \tag{5}$$

$S_{Fe}$ is approximately equal to the soluble ferrous iron concentration, $S_{Fe(II)}$.

$$S_{Fe} = [Fe^{2+}] + [Fe(OH)^+] + [Fe(OH)_{2,aq}] + [Fe(OH)_3^-] \tag{6}$$

The hydrolysis reactions of ferrous ions are shown in Eqs. (7) to (9), where $K_x$ are equilibrium constants [14, 15]. Here the subscript "aq" indicates an aqua complex.

$$Fe^{2+} + H_2O = Fe(OH)^+ + H^+ \qquad\qquad K_1 = [Fe(OH)^+][H^+]/[Fe^{2+}] \tag{7}$$

$$Fe^{2+} + 2H_2O = Fe(OH)_{2,aq} + 2H^+ \qquad\qquad K_2 = [Fe(OH)_{2,aq}][H^+]^2/[Fe^{2+}] \tag{8}$$

$$Fe2+ + 3H2O = Fe(OH)3- + 3H+ \qquad\qquad K_3 = [Fe(OH)_3^-][H^+]^3/[Fe^{2+}] \tag{9}$$

Equation (6) is rewritten using the equilibrium constants as follows.

$$S_{Fe} = [Fe^{2+}](1 + K_1/[H^+] + K_2/[H^+]^2 + K_3/[H^+]^3) \tag{10}$$

The aqua complex concentration, $[Fe^{2+}]$, is limited by the dissolution equilibrium of the stable oxide.

$$3Fe^{2+} + 4H_2O = Fe_3O_4(c) + 6H^+ + H_2 \qquad K_{Fe3O4} = [H^+]^6\,P_{H2}/[Fe^{2+}]^3 \tag{11}$$

$K_{Fe3O4}$ is obtained from change in the Gibbs free energy of the reaction [4, 16].

The hydrogen ion concentration ($[H^+]$) and the hydrogen partial pressure ($P_{H_2}$) in the saturated layer are important parameters for the calculation of $S_{Fe}$. $[H^+]$ was obtained by taking into consideration the dissolution equilibria of $Fe^{2+}$, the hydrolysis equilibria of ammonia and the electric charge balance. $P_{H_2}$ was calculated from $C_{s,H_2}$ using Henry's law. $H_2$ generated by the cathodic reaction diffuses to the bulk solution. Under the steady state in the deaerated solution, the flux of $H_2$ should be the same as the flux of iron [10].

In the presence of DO, the cathodic reaction of oxygen proceeds more rapidly than the cathodic reduction of hydrogen. $C_{s,H_2}$ was calculated by taking into consideration the mass

4

balance of Fe, $H_2$, and $O_2$ at the saturated layer [10]. This FAC model also evaluates the critical DO concentration ($C_{O_2,\text{critical}}$) for FAC suppression [10] as

$$C_{O_2,\text{critical}} = 0.5\, D_{\text{Fe}} \cdot D_{O_2}^{-1} \cdot S_{\text{Fe}}. \tag{12}$$

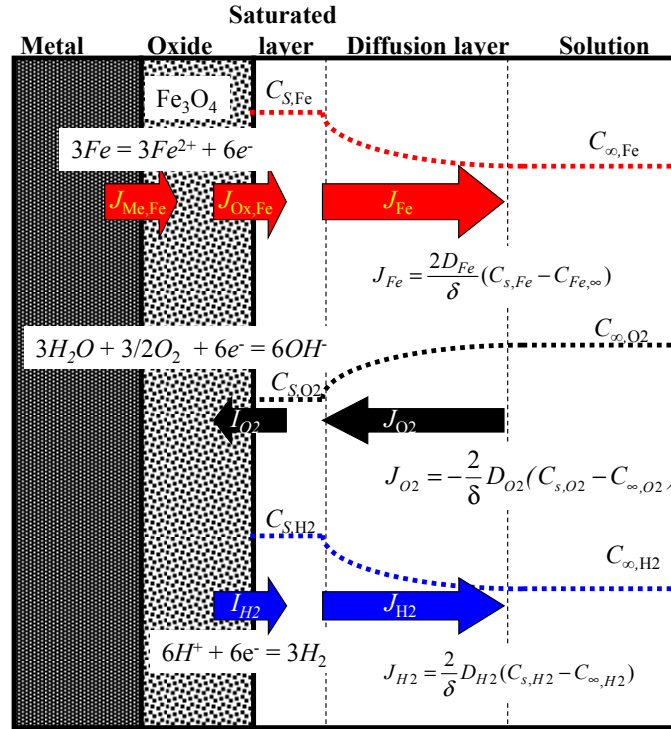From Eq. (12), it is assumed that $C_{O_2,\text{critical}}$ is independent of fluid dynamic parameters.



Figure 3        Model of physicochemical effect on FAC.

## Results

Effect of DO concentration

The DO concentration of the feed water was increased in a stepwise manner during the test run. Figure 4 (a) shows the change in the inner radius during the first test. The DO concentrations in the feed water and outlet water are also shown in the figure. The DO is consumed by the corrosion reaction of carbon steel; thus, the DO concentration in the outlet water is less than that in the feed water. In the neutral solution at 413 K, the change in the inner radius decreased abruptly when the DO concentration was increased to more than 55 ppb. Figure 4 (b) shows the FAC rate evaluated from the change in the inner radius. Although the FAC at a higher velocity was greater than that at a lower velocity, the DO concentration required for FAC suppression was not affected by the velocity.

Figures 5 (a) and (b) show the change in the inner radius during the second test and the FAC rate evaluated from the change in the inner radius, respectively. In the alkaline solution (pH$_{298K}$ 9.2) at 413 K, the change in the inner radius decreased abruptly when the DO concentration was increased to more than 12 ppb, and the DO concentration required for FAC suppression was not affected by the velocity.

Table 3 shows the DO concentration required for FAC suppression obtained from FAC tests. It was clarified that increasing the pH decreases the required DO concentration and that the DO concentration required at 413 K is higher than that at 453 K.
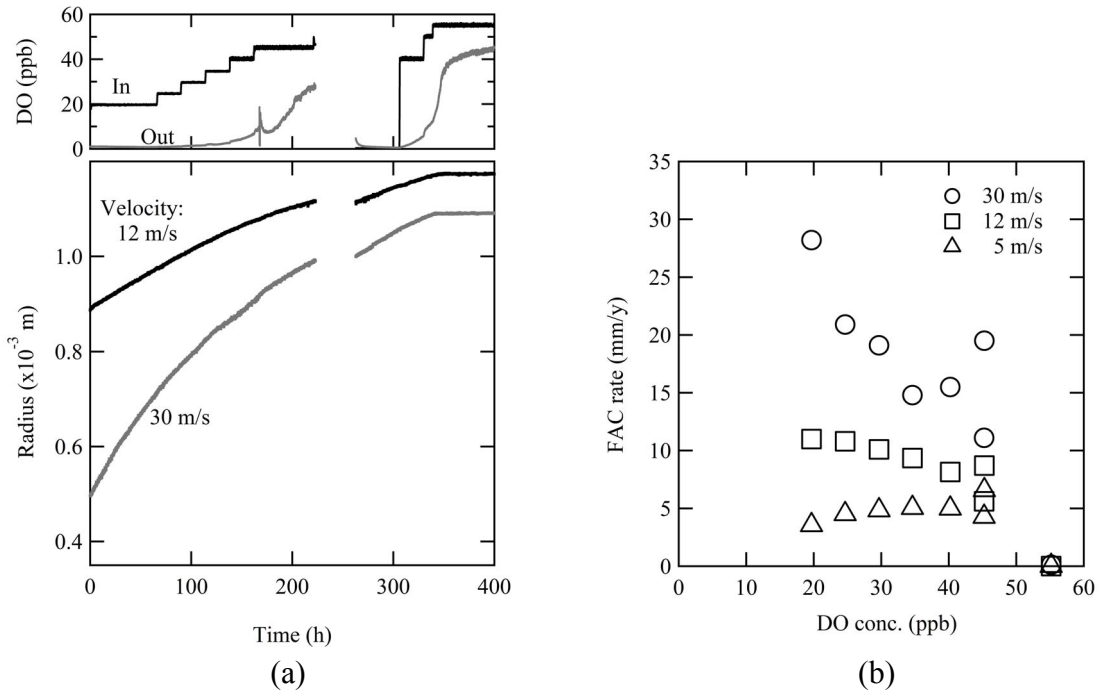
Figure 4　　　Changes in DO concentration and inner radius (a) and relationship between DO concentration and FAC rate (b) obtained from 1st test.
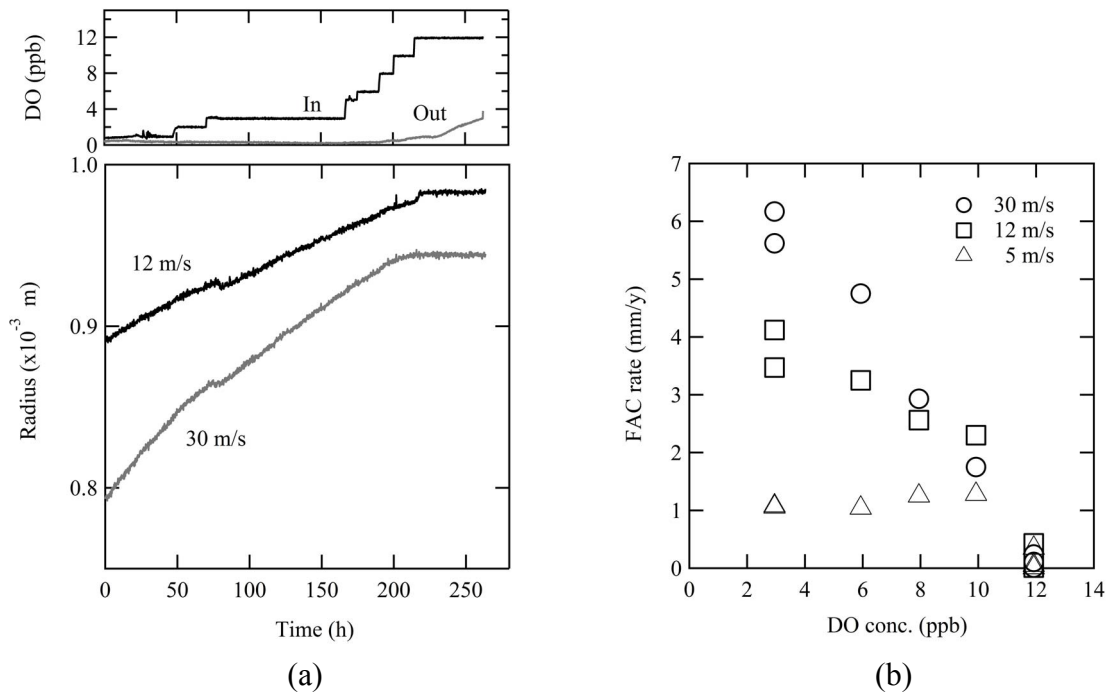


Figure 5　　　Changes in DO concentration and inner radius (a) and relationship between DO concentration and FAC rate (b) obtained from 2nd test.
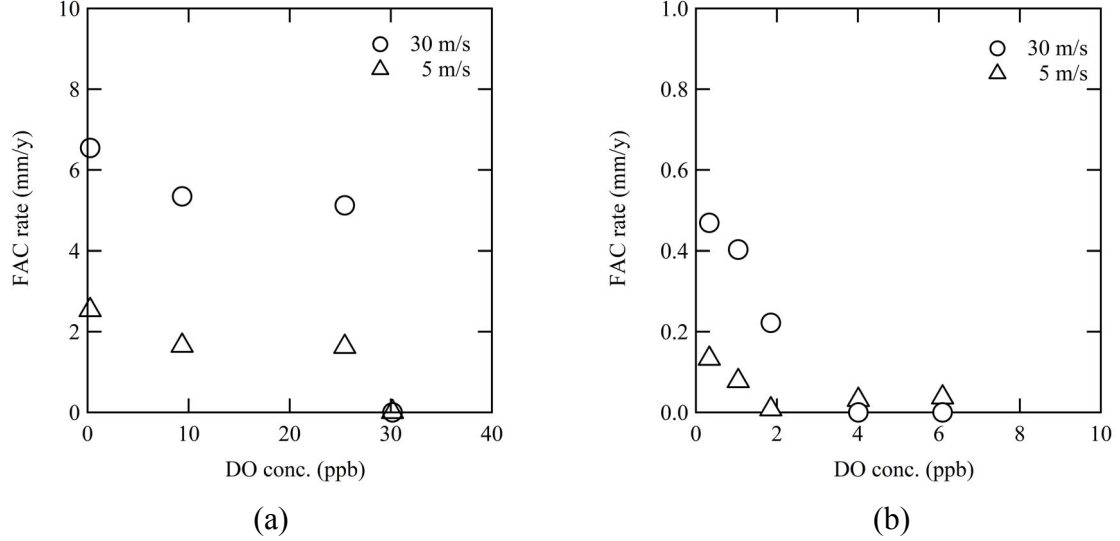
Figure 6    Relationship between DO concentration and FAC rate obtained from 3rd (a) and 4th (b) tests.

Table 3    Comparison of DO concentration required for FAC suppression ($C_{O_2,critical}$).

|  | 413 K | 453 K |
|---|---|---|
| $pH_{298K}$ 7.0 | 50-55 ppb (1st test) | 25-30 ppb (3rd test) |
| $pH_{298K}$ 9.2 | 10-12 ppb (2nd test) | 8 – 10 ppb* |
| $pH_{298K}$ 9.8 | – | 1-4 ppb (4th test) |

*: Result of a test carried out using a different apparatus with a recycling system.

<u>Critical DO concentration for FAC suppression</u>
Table 4 shows $C_{O_2,critical}$ calculated using the FAC model. Although the FAC model can qualitatively explain the experimental results, we encountered some difficulty in quantitative prediction using the FAC model. We considered that one of the factors casing this discrepancy is the uncertainty in $D_{Fe}$. Then $D_{Fe}$ was estimated from the experimental $C_{O_2,critical}$ ($D'_{Fe}$). Table 5 shows the relationship between $D_{Fe}$ and $C_{O_2,critical}$ calculated from Eq. (12). It was clarified that the value of $D_{Fe}$ giving $C_{O_2,critical}$ obtained experimentally was higher than the value of $D_{Fe}$ that we used and that $D_{Fe}$ may be affected by the solution pH.

A change in pH affects the concentration ratios of the dissolved iron species such as $Fe^{2+}$, $Fe(OH)^+$, and $Fe(OH)_2$. Table 6 shows the concentration ratios of $Fe^{2+}$, $Fe(OH)^+$, and $Fe(OH)_2$ in the solution at 453 K. In this study, $D'_{Fe}$ was defined as

$$D'_{Fe} = X_{Fe^{2+}}D'_{Fe^{2+}} + X_{Fe(OH)^+}D'_{Fe(OH)^+} + X_{Fe(OH)_2}D'_{Fe(OH)_2}. \tag{13}$$

Here $D'_{Fe^{2+}}$, $D'_{Fe(OH)^+}$ and $D'_{Fe(OH)_2}$ are the pseudodiffusion coefficients of $Fe^{2+}$, $Fe(OH)^+$, and $Fe(OH)_2$, respectively. All the pseudodiffusion coefficients at 298 K were in the range from $10^{-9}$ to $10^{-8}$ $m^2$/s for the modified model, as shown in Table 7.
Figure 6 shows the FAC rates calculated from the FAC model using $D_{Fe}$ (previous model) and $D'_{Fe}$ (this study). The latter FAC rates and $C_{O_2,critical}$ values are larger than the former. Comparing Figs. 4−5, and 6 with Fig. 7, the FAC rates calculated using the previous model are smaller than the experimental values. For the modified FAC model using $D'_{Fe}$, the

predictive accuracy of the FAC rate was greatly improved. Figure 8 shows the effect of the temperature and $pH_{298K}$ on the FAC rate calculated using the modified FAC model. The effect of the temperature on the FAC rate changes with $pH_{298K}$. The temperature at which the FAC rate is maximum is higher in the alkaline solution with $pH_{298K}$ 9.2 than in the neutral solution with $pH_{298K}$ 7. At 413 K, when $pH_{298K}$ of the solution exceeds about 8.5, the FAC rate drops abruptly. The quantitative validity of these behaviors should be confirmed by further experiments, and the FAC model should be further modified.

Table 4    $C_{O_2,critical}$ calculated by FAC model using constant $D_{Fe}$.

|  | 413 K | 453 K |
|---|---|---|
| $pH_{298K}$ 7.0 | 8.5 ppb | 5.6 ppb |
| $pH_{298K}$ 9.2 | 0.6 ppb |  |
| $pH_{298K}$ 9.8 | – | 0.1 ppb |

Table 5    Relationship between $D_{Fe}$ at 298 K and $C_{O_2,critical}$ at 453 K.

| $D_{Fe}$ (at 298 K) (m²/s) | $D_{Fe}$ (at 453 K) (m²/s) | $C_{O_2,critical}$ (ppb) | | |
|---|---|---|---|---|
|  |  | $pH_{298K}$ 7 | $pH_{298K}$ 9.2 | $pH_{298K}$ 9.8 |
| 8.42E-10 | 7.55E-09 | 5.6 | 0.6 | 0.08 |
| **3.30E-09** | 2.96E-08 | **29.0** | 4.1 | 0.6 |
| **5.50E-09** | 3.43E-08 | 53.0 | **8.6** | 1.3 |
| **7.30E-09** | 6.55E-08 | 74.0 | 13.2 | **1.9** |

Table 6    Concentration ratios ($X_y$) of soluble Fe(II) species in the solution at 453 K.

|  | $X_{Fe^{2+}}$ | $X_{Fe(OH)^+}$ | $X_{Fe(OH)_{2,aq}}$ |
|---|---|---|---|
| $pH_{298K}$ 7.0 | 0.719 | 0.276 | 0.005 |
| $pH_{298K}$ 9.2 | 0.321 | 0.623 | 0.056 |
| $pH_{298K}$ 9.8 | 0.105 | 0.686 | 0.209 |

Table 7    $D'_{Fe^{2+}}$, $D'_{Fe(OH)^+}$ and $D'_{Fe(OH)_2}$ at 298 K.

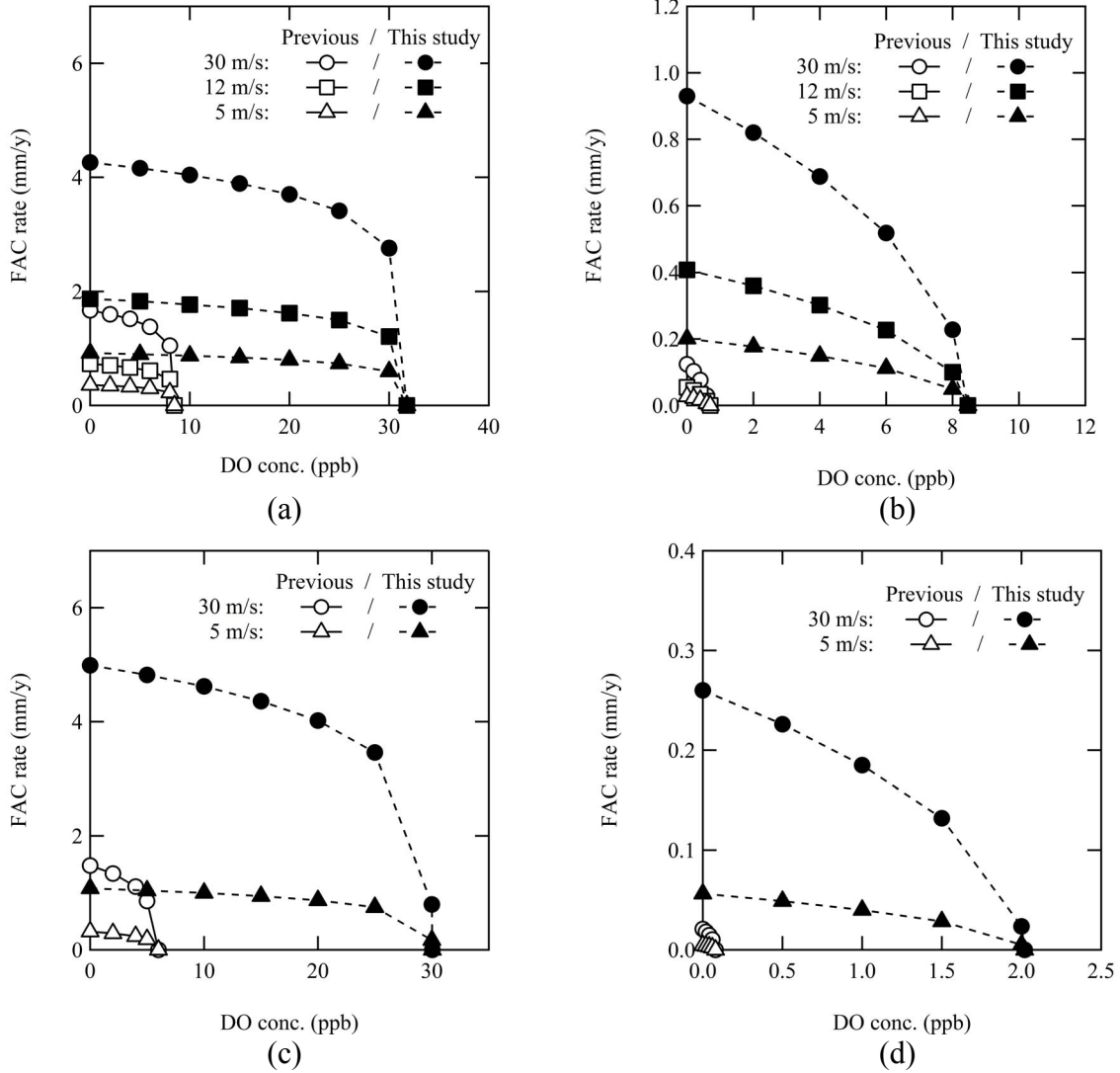|  | $D'_{Fe^{2+}}$ (at 298 K) (m²/s) | $D'_{Fe(OH)^+}$ (at 298 K) (m²/s) | $D'_{Fe(OH)_2}$ (at 298 K) (m²/s) |
|---|---|---|---|
| Original model | 8.42E-10 | - | - |
| Modified model | 2.09E-09 | 6.67E-09 | 1.20E-08 |

Figure 7    FAC rates calculated using the previous and modified FAC models: (a) 413 K, pH$_{298K}$ 7.0, (b) 413 K, pH$_{298K}$ 9.2, (c) 453 K, pH$_{298K}$ 7.0, and (d) 453 K, pH$_{298K}$ 9.8.
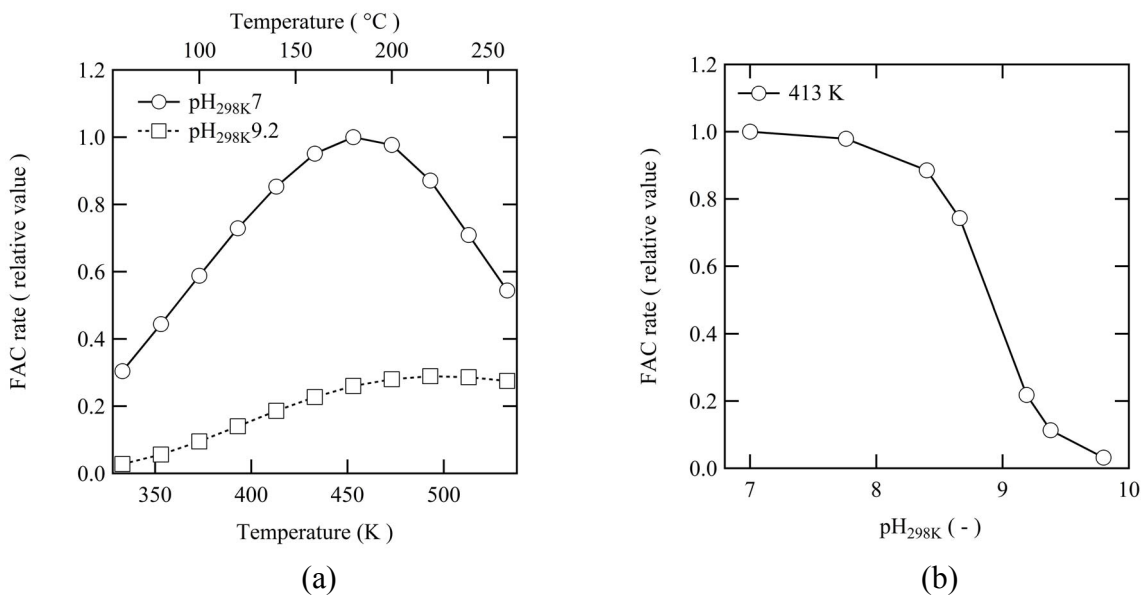


Figure 8    Effects of temperature (a) and pH$_{298K}$ (b) on FAC rate calculated usingy modified FAC model.

## Conclusion

The effect of DO on the FAC rate was experimentally evaluated in neutral and alkaline solutions at 413 and 453 K. In the neutral ($pH_{298K}$ 7.0) and alkaline solutions ($pH_{298K}$ 9.2) at 413 K, the FAC was suppressed when the DO concentration was increased to more than 55 and 12 ppb, respectively. At 453 K, the DO concentration required for FAC suppression was more than 30 and 4 ppb in the neutral solution ($pH_{298K}$ 7.0) and alkaline solution ($pH_{298K}$ 9.8), respectively. The DO concentration required for FAC suppression was not affected by the flow velocity according to result predicted by the FAC model. However, it was higher than the value predicted by the FAC model. It was assumed that the discrepancy between the experimental and predicted results was caused by the uncertainty in the diffusion coefficient of soluble iron and that the diffusion coefficient was affected by the distribution of soluble ferrous species. The modification of the diffusion coefficient improved predictive accuracy of FAC rate.

## References

1. H. G. Heitmann and P. Schub, Proc. Water Chemistry of Nuclear Reactor System 3 Vol.1, BNES, London, U.K., 1983, pp. 243-252.
2. G. J. Bignold, K. Garbett, R. Garnsey and I. S. Woolsey, Proc. Water Chemistry of Nuclear Reactor System 2, BNES, London, U.K., 1980, pp. 5-18.
3. V. H. G. Heitmann and W. Kastner, VGB-Kraftwerkstechnik, 62 (1974) pp. 211-219.
4. Atomic Energy Society of Japan, Handbook of Water Chemistry of Nuclear Reactor System, Corona Publishing Co., Ltd., Tokyo, Japan, 2000. (in Japanese)
5. M. Izumiya, F. Mizuniwa, K. Osumi, T. Kanbayashi, Y. Matsushima, and K. Tanno, Karyoku Genshiryoku Hatsuden, 27 (1976) pp. 419-426. (in Japanese)
6. K. Fujiwara, M. Domae, T. Ohira, K. Hisamune, H. Takiguchi, S. Uchida, and D. Lister, Proc. 16th Pacific Basin Nuclear Conference, AESJ, Tokyo, Japan, 2008, Paper No. P16P1048.
7. O. D. Bouvier, M. Bouchacourt and K. Fruzzetti, Proc. Chimie 2002 Water Chemistry in Nuclear Reactor System, SFEN, Paris, France, 2002, Paper No. 117.
8. I. S. Woolsey, G. J. Bignold, C. H. D. Whalley, and K. Garbett, Proc. Water Chemistry of Nuclear Reactor System 4, BNES, London, U.K., 1986, pp. 337-346.
9. D. H. Lister, L. Liu, A. D. Feicht, M. Khatibi, W. G. Cook, K. Fujiwara, E. Kadoi, T. Ohira, H. Takiguchi, and S. Uchida, PowerPlant Chem., 10 (2008), pp. 659-667.
10. K. Fujiwara, M. Domae, K. Yoneda, and F. Inada, Corros. Sci., 53, 11(2011), pp. 3526-3533.
11. K. Fujiwara, M. Domae, K. Yoneda, F. Inada, T. Ohira, and K. Hisamune, Nuclear Engineering and Design, 241, 11(2011), pp. 4482-4486.
12. K. Fujiwara, M. Domae, K. Yoneda, and F. Inada, NPC2010, Quebec, Canada, 6.06P, 2010
13. T. H. Chilton, and A. P. Colburn, Ind. Eng. Chem., 26 (1934), pp. 1183-1187.
14. J. W. Cobble, R. C. Murray, Jr., P. J. Turner and K. Chen, EPRI NP-2400 (1982).
15. F. H. Sweeton, and C. F. Base, J. Chem. Thermodyn., 2, p. 479 (1970).
16. Thermodynamic Database MALT Group, Thermodynamic Database MALT for Windows, Kagaku Gijutsu-Sha, Tokyo, Japan, 2005. (CD-ROM)